Crack Branching and Fracture Mirror Data of Glasses and Advanced Ceramics

Sung R. Choi
Cleveland State University, Cleveland, Ohio

John P. Gyekenyesi
Lewis Research Center, Cleveland, Ohio

The NASA STI Program Office ... in Profile

Since its founding, NASA has been dedicated to the advancement of aeronautics and space science. The NASA Scientific and Technical Information (STI) Program Office plays a key part in helping NASA maintain this important role.

The NASA STI Program Office is operated by Langley Research Center, the lead center for NASA's scientific and technical information. The NASA STI Program Office provides access to the NASA STI Database, the largest collection of aeronautical and space science STI in the world. The Program Office is also NASA's institutional mechanism for disseminating the results of its research and development activities. These results are published by NASA in the NASA STI Report Series, which includes the following report types:

- TECHNICAL PUBLICATION. Reports of completed research or a major significant phase of research that present the results of NASA programs and include extensive data or theoretical analysis. Includes compilations of significant scientific and technical data and information deemed to be of continuing reference value. NASA counter-part of peer reviewed formal professional papers, but having less stringent limitations on manuscript length and extent of graphic presentations.

- TECHNICAL MEMORANDUM. Scientific and technical findings that are preliminary or of specialized interest, e.g., quick release reports, working papers, and bibliographies that contain minimal annotation. Does not contain extensive analysis.

- CONTRACTOR REPORT. Scientific and technical findings by NASA-sponsored contractors and grantees.

- CONFERENCE PUBLICATION. Collected papers from scientific and technical conferences, symposia, seminars, or other meetings sponsored or co-sponsored by NASA.

- SPECIAL PUBLICATION. Scientific, technical, or historical information from NASA programs, projects, and missions, often concerned with subjects having substantial public interest.

- TECHNICAL TRANSLATION. English-language translations of foreign scientific and technical material pertinent to NASA's mission.

Specialized services that help round out the STI Program Office's diverse offerings include creating custom thesauri, building customized databases, organizing and publishing research results ... even providing videos.

For more information about the NASA STI Program Office, you can:

- Access the NASA STI Program Home Page at http://www.sti.nasa.gov/ STI-homepage.html

- E-mail your question via the Internet to help@sti.nasa.gov

- Fax your question to the NASA Access Help Desk at (301) 621-0134

- Phone the NASA Access Help Desk at (301) 621-0390

- Write to:
  NASA Access Help Desk
  NASA Center for AeroSpace Information
  800 Elkridge Landing Road
  Linthicum Heights, MD 21090-2934

Crack Branching and Fracture Mirror Data of Glasses and Advanced Ceramics

Sung R. Choi
Cleveland State University, Cleveland, Ohio

John P. Gyekenyesi
Lewis Research Center, Cleveland, Ohio

National Aeronautics and
Space Administration

Lewis Research Center

February 1998

Available from

CRACK BRANCHING AND FRACTURE MIRROR DATA OF GLASSES AND ADVANCED CERAMICS

Sung R. Choi[*]
Cleveland State University
Cleveland, Ohio 44115

and

John P. Gyekenyesi
National Aeronautics and Space Administration
Lewis Research Center
Cleveland, Ohio 44135

SUMMARY

The fracture mirror and crack branching constants were determined from three glasses and nine advanced ceramics tested under various loading and specimen configurations in an attempt to use the constants as a data base for fractography. The ratios of fracture mirror or crack branching constant to fracture toughness were found to be approximately two for most ceramic materials tested. A demonstration of how to use the two constants as a tool for verifying stress measurements was presented for silicon nitride disk specimens subjected to high-temperature, constant stress-rate biaxial flexure testing.

I. BACKGROUND

Fractographic analysis of glasses and ceramics can play an essential role in not only locating and characterizing fracture origins but identifying failure mechanisms. The commonly observed features of brittle fracture are mirror, mist, hackle, and crack-branching patterns which are normally formed in fracture surfaces particularly for silicate glasses, as shown in figure 1 (ref. 1). As a crack propagates catastrophically from its origin, it leaves behind sequentially these distinctive surface features. These fracture features with their boundaries can give significant information as well as empirical practicality in failure analysis. Fracture mirrors have been utilized to pinpoint fracture origins, to predict the sizes of failure-initiating flaws, to estimate fracture stresses, and to determine residual stresses presented in specimens (refs. 1 to 7). In terms of analytical approach, however, an enormous complexity has been encountered in understanding and formulating the mechanics of these fracture features with respect to dynamic crack propagation.

The distances from the fracture origin to the boundaries (fig. 1) have been empirically related with the fracture strength as follows (refs. 1 and 8)

$$\sigma_f r_i^{1/2} = A_i \tag{1}$$

where σ_f is the fracture strength (typically in MPa), r_i is the radius of the ith boundary from the fracture origin (typically in meter) and A_i is the constant for the ith boundary. Note that the units of A, $\mathrm{MPa\sqrt{m}}$, are the same as those of stress intensity factor. The parameter A_m is known as the fracture mirror constant for the boundary of the mirror and the mist regions, and the parameter A_b is the crack branching constant for the boundary of the hackle

---

[*]NASA Senior Resident Researcher at Lewis Research Center, Cleveland, Ohio 44135.

and the branching regions. In some cases, particularly for polycrstalline ceramics, fracture mirror size (r_m) and crack branching length (r_b) are not clearly distinguishable so that little difference between the fracture mirror and the crack branching constants has been attained.

Many investigations have been made to determine the fracture mirror or crack branching constant for silicate glasses since these materials generally exhibit the four distinctive fracture features, allowing reasonably accurate measurements of mirror sizes or crack branching lengths. The fracture mirror constant or crack branching constant has appeared to range from $A = 1.7$ to 2.7 MPa$\sqrt{m}$ with an approximate mean of $A = 2$ MPa$\sqrt{m}$, regardless of flaw history such as modes of loading (flexure or tension, uniaxial or biaxial), residual contact stresses, and environment (refs. 1 and 4 to 11). Because of this somewhat consistent result, the constant has been combined with fracture toughness of the material, drawing a conclusion that the constant would be a unique material constant. However, the scatter of mirror constants available in the literature is not comparable with that of mechanical properties such as fracture toughness, hardness and Young's modulus. The mirror constants have shown a greater variation depending on load/specimen configurations and even on investigators than fracture toughness, hardness or Young's modulus. By contrast, for example, fracture toughness of soda-lime and fused silica glasses do not exhibit any appreciable variation in terms of test method which is either by indentation, double torsion, double cantilever beam, compact tension, single edge precracked beam or by any other test techniques, with a range of $K_{IC} = 0.75$ to 0.79 MPa$\sqrt{m}$, as pointed out by Ramulu (ref. 12). Particularly for polycrystalline ceramics in which the respective boundaries are not generally well defined, the variation in A has become more significant (refs. 1, 4, 10, and 13).

Because of the inconsistency in A, some investigators have pointed out that fracture mirror or crack branching constant is not merely a material constant. In his dynamic fracture mechanics analysis using a dynamic finite element method, Ramulu (ref. 12) has shown that the formation of fracture mirror for soda-lime glass is attributed to the oscillations of dynamic stress intensity factor ($= K_{ID}$) as a crack propagates rapidly, suggesting that the constant be a product of mechanics response. Although several criteria such as velocity (ref. 14), strain energy density (refs. 8 and 9) and static stress intensity factor (refs. 15 to 18) have been proposed and each criterion is suitable to a certain specific condition, none of the criterion can explain satisfactorily all the detailed mechanics on the formation of fracture mirror and subsequent features (ref. 1). This is due to limited understanding of dynamic crack propagation in the nature of catastrophic failure associated with stress wave interaction, which has been considered as a 'formidable' problem.

Notwithstanding the difficulty in understanding the exact nature (mechanics) of fracture-mirror formation, the fracture mirror or crack branching constant has been used widely as a tool to predict the flaw size as well as the fracture stress associated with failure, as aforementioned. In some cases, critical flaws are too small in size to measure even microscopically and/or are not discernable enough to characterize their configurations. In this case, the fracture mirror sizes and mirror constant can give a useful information to estimate the flaw sizes at failure. Based on the fracture mechanics approach together with equation (1), a ratio of mirror size to critical flaw size can be obtained for an infinite body as follows:

$$\frac{r_m}{c_f} = \left(\frac{K_m}{K_{IC}}\right)^2 \tag{2}$$

where K_m is the 'stress intensity factor' at mirror formation, expressed as $K_m = Y\sigma_f r_m^{1/2} = YA_m$ with Y being a crack geometry factor, and $K_{IC} = Y\sigma_f c_f^{1/2}$ with c_f being a critical crack size. For example, a ratio of mirror size to flaw size was found to be about $c_f/r_m = 10$ to 13 for silicate glasses (ref. 2). In other cases, a situation may occur where a ceramic component has failed in service without the working stress being known. If it is feasible to determine fracture mirror size or crack branching length through fractography, the approximate operating-stress that had caused the component to fail can be estimated based on equation (1) with the fracture mirror or crack branching constant available. Consequently, any pertinent changes in design or operating conditions would be made through this post-failure analysis. Since a failure-initiating flaw is generally surrounded symmetrically by mirror, mist and hackle regions (fig. 1), the location of the flaw also can be easily identified. In summary, the data on fracture mirror and/or crack-branching, sizes and constants, can be utilized very usefully in fractographic analysis of brittle materials. An ASTM standard (C 1322) (ref. 19) for fractographic analysis of advanced ceramics describes this technique in details, and many review articles on fractography allocate a large portion for the features of fracture-mirror or crack-branching sizes and constants, which reflect both the importance and usefulness of the technique.

A large quantity of glass and ceramic specimens have been tested under various testing programs at the Ceramics Lab of NASA Lewis Research Center. The measurements on fracture mirror sizes and/or crack branching lengths have been made for some of these glass and advanced ceramic specimens tested in constant stress-rate or strength testing at either room or elevated temperatures. This paper summarizes the measurements of fracture mirror sizes and/or crack branching lengths as a function of fracture stress for three glasses and nine advanced ceramics to determine the corresponding fracture mirror and/or crack branching constants. Since, in general, the fracture mirror or crack branching constants have shown to vary depending on materials, test methods and/or specimen confugurations, a large amount of data covering a variety of test matrices is needed. The determined constants can then be used as a data base for a wide range of materials and/or specimen/loading configurations. Finally, an example of how fracture stresses were able to be remedied by the use of fractographic analysis based on equation (1) is presented for silicon nitride specimens subjected to uniaxial and biaxial flexure testing at elevated temperature.

II. EXPERIMENTS

Types of testing, and loading and specimen configurations for each test material where the measurements of fracture mirror size or crack branching length were attained, are summarized in Table I. The table also includes hardness, fracture toughness, fracture mirror or crack branching constant, ratio of fracture mirror or crack branching constant to fracture toughness of each material. Due to the variety of test matrices, detailed experimental procedures for each material were omitted here and should be referred to the corresponding reference. Brief descriptions regarding test conditions and specimens were made in the Result and Discussion section. The mirror sizes and crack branching lengths were determined using low power microscopes, typically ranging in magnification from 10 times to 100 times. In general, the measurements of fracture mirror sizes were made for the specimens tested in uniaxial tension or uniaxial flexure, while the measurements of crack branching lengths were made for the disk or plate specimens in biaxial flexure. Exception to this was soda-lime glass plates (microslides) where fracture mirror sizes and crack branching lengths were determined, respectively, from biaxial and uniaxial flexure.

III. RESULTS AND DISCUSSION

1. Fracture Mirror and Crack Branching

(a) NC132 silicon nitride in uniaxial and biaxial flexures

Figure 2 shows the plots of fracture stress (log σ_m) as a function of fracture mirror size (log r_m) (fig. 1(a)) and of crack branching length (log r_b) (fig. 1(b)). This figure is for NC 132 silicon nitride uniaxial (four-point beam) and biaxial (ring-on-ring disk) flexural specimens subjected to constant stress-rate (or called "dynamic fatigue") testing at 1100 °C in air (ref. 20). The mirror and branching constants were determined to be $A_m = 9.40 \pm 1.19$ MPa$\sqrt{m}$ and $A_b = 5.66 \pm 1.49$ MPa$\sqrt{m}$, respectively, from the functional-fit analysis based on equation (1). Contrary to common observations, the crack branching constant was rather small (40 percent less), as compared with the mirror constant. This was due to the error in fracture-stress measurements in biaxial flexure, which will be discussed in the later section. A typical fracture surface of a uniaxial four-point bar specimen as well as a typical crack branching pattern of a biaxial disk specimen is shown in figure 3.

(b) GN10 silicon nitride in pure tension and biaxial flexure

Figure 4 depicts both the fracture stress plotted versus fracture mirror size for GN10 button-head, pure tension specimens (ref. 21) and the fracture stress as function of crack branching length for GN10 particle-impacted, biaxial disk specimens (ref. 22). The mirror constant in pure tension was $A_m = 11.78 \pm 1.41$ MPa$\sqrt{m}$, and the crack branching constant in biaxial flexure was $A_b = 10.32$ MPa$\sqrt{m}$. Despite different vintage, a reasonable agreement between the two constants exists, indicating that the constants for GN10 are almost independent of flaw history with either machined surface with monotonic tension loading or particle-impacted surface with biaxial flexure

loading. The independence of fracture mirror or crack branching constant on flaw history such as flaw type, loading condition and environment has been observed for many glasses and advanced ceramics (refs. 1 and 4 to 11). It should be noted that the demarcation between mirror and hackle regions is not usually well-defined in polycrstalline ceramics so that the difference between A_m and A_b is insignificant (refs. 10 and 13).

(c) Hexoloy silicon carbide in biaxial flexure

The crack branching results for Hexoloy silicon carbide (α – SiC) plates tested in ring-on-ring biaxial flexure (ref. 23) are shown in figure 5. The branching constant was $A_b = 5.45 \pm 0.30$ MPa$\sqrt{m}$ for a total of 111 data points resulting in an excellent data fit to equation (1) with a coefficient of variation of 5 percent in A_b. A typical crack branching pattern and a corresponding fracture surface of a tested specimen are shown in figure 6. It is noted that the surface flaw yielded a through-the-thickness crack that extended in a plane to a length of $2r_b$ before branching into several segments, as observed in biaxial disk fracture by Shetty et al. (ref. 24).

(d) 96 wt% alumina in uniaxial and biaxial flexures

The results for the crack-branching length and fracture-mirror size measurements for 96 wt% alumina in four-point uniaxial, ring-on-ring biaxial and ball-on-ring biaxial flexures (ref. 25) are shown in figure 7. The constants were found to be $A_m = 7.64 \pm 0.53$ and $A_b = 7.24 \pm 0.66$ and 7.39 ± 0.55 MPa$\sqrt{m}$, respectively, for four-point uniaxial, ring-on-ring biaxial and ball-on-ring biaxial flexures. Little variation in A's among the three different test conditions indicates again the independence of A on flaw, specimen and/or loading configurations.

(e) Y-TZP, AS44 and SN220 silicon nitrides in biaxial flexure

The post-impact strength as a function of crack branching length for Y-TZP, AS44 and SN220 silicon nitride disk specimens are depicted in figure 8. Each disk specimen was subjected to a specified particle-impact test and then its subsequent strength was determined by using a ring-on-ring biaxial fixture at room temperature (ref. 22). The crack branching constants were $A_b = 11.48 \pm 1.46$, 10.85 ± 2.71, and 8.13 ± 2.36 MPa$\sqrt{m}$, respectively, for Y-TZP, AS44 and SN220. It is noted that the scatter in the data was significant at high r_b, particularly for AS44 and SN220 silicon nitrides. It is questionable whether the crack branching data with $r_b \geq 1$ mm can be included, in view of equation (1) which is based on the assumptions of an infinite body and a uniaxial stress-state. However, the values of crack branching constant excluding such data ($r_b \geq 1$ mm) would not be appreciably different from those for all data included.

(f) SiC whisker-reinforced composite silicon nitride and monolithic silicon nitride in uniaxial flexure

The previously published, fracture stress versus mirror size data on 30 vol% SiC whisker-reinforced composite silicon nitride and similar monolithic silicon nitride (both fabricated by Norton Co.) (ref. 13) are presented in figure 9. The strengths of both the composite and monolithic (flexure beam) specimens indented with indentation loads (with Vickers microhardness indenter) ranging from 1 to 10 N were determined in four-point flexure at room temperature. The fracture mirror constant was $A_m = 6.63 \pm 0.11$ and 5.88 ± 0.14 MPa$\sqrt{m}$, respectively, for the composite and monolithic silicon nitrides.

(g) Glasses in uniaxial and biaxial flexures and in pure tension

The results of fracture stress vs. mirror size for different glasses are shown in figure 10. The figure consists of the data on: (a) fused silica rods (as-received) in four-point uniaxial flexure (ref. 26); soda-lime glass square plates (annealed and etched) in ring-on-ring biaxial flexure (ref. 27); and indented fused silica optical glass fibers (ref. 7). The mirror constant was obtained to be $A_m = 2.20 \pm 0.33$, 1.81 ± 0.28, and 2.10 MPa$\sqrt{m}$, respectively, for fused silica rods, soda-lime square plates, and optical glass fibers. The values of fracture mirror constant are in good agreement with the published data which range from $A_m = 1.7$ - 2.7 MPa$\sqrt{m}$ with a mean of $A_m = 2$ MPa$\sqrt{m}$ (refs. 1 and 4 to 1). This indicates again that the mirror constant for glass is almost independent of the flaw history

such as loading (pure tension, or uniaxial or biaxial flexure), flaw types (natural, machining or indentation flaws) and environment (moisture or inert), as long recognized (refs. 1 and 4 to 11). A typical fracture surface of a fused silica glass rod showing a well-defined mirror formation is shown in figure 11.

The crack branching data on soda-lime glass rectangular plates subjected to constant stress-rate testing in four-point flexure were purposely collected and are presented in figure 12. The specimens were indented with low indentation loads (P = 2 and 5 N with Vickers microhardness indenter), and tested in as-indented or annealed condition (ref. 28). The crack branching constant was found to be $A_b = 3.54 \pm 0.64$ MPa$\sqrt{m}$. This value of crack branching constant is considerably higher than those shown in figure 10. Also note a poor data fit to equation (1) with a coefficient of variation of 18 percent in A_b. The figure shows that the lower r_b's yield the lower branching constant, and *vise versa*. This clearly indicates that there exists a lower limit of branching length (in conjunction with specimen thickness) below which only a reasonable value of crack branching constant is obtained. Therefore, the use of equation (1) to determine the crack branching constant for branching lengths greater than 1 mm for thin (1.2 mm thick) microslides is not appropriate, primarily due to the inapplicability of the infinite-body assumption. Typical crack branching patterns and corresponding fracture surfaces for the two specimens failed at low and high fracture stresses are shown in figure 13. Simialr to figure 6, the surface flaws extended in a plane to almost a length $2r_b$ to form through-the-thickness cracks before branching.

2. The Ratio of Fracture Mirror or Crack Branching Constant to Fracture Toughness, A/K_{IC}

A summary of the ratios of fracture mirror or crack branching constant to fracture toughness, A/K_{IC}, is presented in Table I. The plots of A as a function of K_{IC} are also shown in figure 14. Here, the soda-lime glass uniaxial flexure data (fig. 12) were not included since some of crack branching lengths were much greater than the specimen thickness. The NC132 fracture mirror constant was corrected with a correction factor of 1.38 (see Section 4). Glasses exhibit the ratios ranging from $A/K_{IC} = 2.4$ to 2.8. However, most other data except for glasses seem to follow approximately along the line of $A/K_{IC} \approx 2$, with an overall average value of $A/K_{IC} = 2.05 \pm 0.34$. This is somewhat inconsistent with the results obtained by Rice et al. (refs. 2 and 6), where the data follow reasonably well with a ratio of $A/K_{IC} \approx 3$. However, it should be noted that a relatively large range of the ratios from $A/K_{IC} = 1.1$ to 3 has been reported for polycrystalline ceramics, depending on specimens, loading configurations and even researchers (refs. 10, 13, and 19). This implies that the ratio is not solely a material-independent constant for advanced ceramics, as pointed out previously (refs. 10, 12, and 13), which in turn means fracture mirror or crack branching constant is not a uniquely-defined material constant. This is in contrast with other physical properties such as Young's modulus and fracture toughness. It is believed that the discrepancy may be further amplified particularly for the fracture mirror constant, due to the arbitrary choice of mirror boundaries in polycrystalline ceramics since unlike glasses the boundaries are not completely evident (refs. 10 and 13).

3. Effect of Hardness on Crack Branching

Kirchner suggested that a critical crack-tip strain should be reached to initiate branching (ref. 29). The basic idea is that crack branching occurs when the total strain at the boundary of a yield zone at the crack tip is a constant that is related to the crack opening required for a branching crack in ceramics, and that hardness is a factor in determining the crack tip strain. With some ceramics data Kirchner showed a relationship between stress intensity factor and hardness of the material as follows:

$$K_B = MH + \sqrt{2K_{IC}} \qquad (3)$$

where K_B is the (static) stress intensity factor at branching, expressed as $K_B = Y\sigma_f r_B^{1/2} = YA_B$, H is hardness, and M is a constant (or the slope in a plot of K_B versus H). The crack geometry factor Y does not change more than 10 percent in the range of $0 \leq r_B \leq 0.5t$ with t being specimen thickness (ref. 30). Equation (3) also can be used by replacing K_B with A_B (or A_m) since the functional trend remains unchanged. The results of A/K_{IC} versus H/K_{IC} for glasses and ceramics are shown in figure 15. The soda-lime glass crack branching data shown in figure 12 was not included in the figure. The NC132 fracture mirror constant was corrected with a correction factor of 1.38 (see

Section 4). Unlike the data shown by Kirchner (ref. 29), a significant scatter is apparent in the data obtained from this study, as shown in the figure. Notwithstanding, overall trends suggested by Kirchner seem to be supported by much broader range of dada, as also mentioned by Rice (ref. 1).

It has been shown that the commonly referred three criteria of fracture mirror formation or crack branching, crack velocity, strain energy density and stress intensity factor, are generally interrelated. Rice mentioned that for example, crack velocity is generally related to both strain energy density and stress intensity factor; in turn, strain energy density can be directly related to stress intensity factor, and Kirchner's strain intensity criterion is a direct algebraic derivative of the stress intensity factor criterion (ref. 1). This means that taken separately, none of the criterion can give a satisfactory explanation to all of the observations made earlier. In fact, one of the basic difficulties with previous explanations is their attempt to explain all phenomena by a single criterion. Instead, two or more criteria may be required for explaining the fracture phenomena, as detailed by Rice (ref. 1).

4. Application of Fracture Mirror and/or Crack Branching Constants for the Appropriateness of Stress Measurements

The uniaxial and biaxial flexural strengths of NC132 silicon nitride were previously determined in constant stress-rate testing at 1100 °C in air (ref. 20). The biaxial strength predicted from the uniaxial strength data, based on the Weibull statistics, was substantially higher (60 percent) than the actual biaxial data. This prompted a fractographic analysis to determine both the fracture mirror constant for the rectangular beam specimens tested in uniaxial flexure and the crack branching constant for the disk specimens tested in biaxial flexure. The idea came from the fact that regardless of flaw history (flaw type, stress state, or environment) the crack branching constant of a given material is not greatly different from the fracture mirror constant. Therefore, by comparing the two constants, the appropriateness of the stress measurements determined from each individual testing can be verified. The fracture mirror and crack branching constants were obtained as $A = 9.40 \pm 1.19$ and 5.66 ± 1.49 MPa$\sqrt{\text{m}}$, respectively, which is already shown in figure 2. This value of fracture mirror constant is significantly higher (66 percent) than the crack branching constant. This indicates that in order to have a value of crack branching constant similar to that of fracture mirror constant, the stress determined in the biaxial specimens would need to have been increased by at least 66 percent (eq. (1)).

Several approaches were made to pinpoint the reason for discrepancy in the stress measurements occurring in biaxial flexure (ref. 20). They included analytical stress calculation, indentation strength method and strain-gaging experiments to determine the related stresses of the biaxial disk specimens. Details regarding these approaches can be found in a previous report (ref. 20). Based on the results of these three approaches, it was found that the desirable state of biaxial stress could not be achieved within the loading-ring diameter of a disk specimen for a given number of loading balls of five (for the upper fixture). The stress occuring at the tensile side of a disk specimen, responsible for fracture, was highest on the loading-ball site (region 'A'), intermediate at the center (region 'C') and lowest between the two adjacent loading balls (region 'B') (fig. 16). Therefore, the strengths obtained from the disk specimens were underestimated since the stress calculation was based on the magnitude occurring at the center of the specimen (ref. 24). Most of the disk specimens failed from the regions (region 'A') directly under the loading balls. Therefore, the obtained failure stress should be modified with an appropriate correction factor. A correction factor of 1.38 was determined from the results of these three approaches. The correction factor of 1.38 yielded a new fracture mirror constant of $A_m = 7.81$ MPa$\sqrt{\text{m}}$, which is in reasonable agreement with $A_b = 9.40$ MPa$\sqrt{\text{m}}$. This also gave a much better prediction in strength between the uniaxial and biaxial loading conditions. It was found that a reasonably accurate biaxial state of stress within the loading-ring diameter can be obtained by using an increased number of loading balls (at least or greater than 10). Furthermore, it was found that a continuous ring-on-ring configuration with a condition of minimized friction provides another alternative for a proper biaxial strength testing method. A fractographic analysis using the fracture mirror and crack branching constants thus can be utilized as an efficient tool to identify the problem associated with stress measurements, which was demonstrated with the uniaxial and biaxial flexural strength data obtained from high-temperature, constant stress-rate testing for NC132 silicon nitride.

IV. CONCLUSIONS

The fracture mirror and crack branching constants were determined for glasses and advanced ceramics tested under various loading and specimen configurations in an attempt to utilize the constants as a data base on fractography. The ratios of fracture mirror or crack branching constant to fracture toughness were found to be approximately two for most ceramic materials tested. A demonstration to use the two constants as a verification tool for the appropriateness of stress measurements was made for silicon nitride disk specimens subjected to high-temperature, constant stress-rate testing.

ACKNOWLEDGMENTS

REFERENCES

1. R. W. Rice, "Perspective on Fractography," pp. 3-56 in Fractography of Glass and Ceramics, Advanced in Ceramics, vol. 22, edited by J. R. Varner and V. D. Frechette, The American Ceramic Society, 1988.

2. J. J. Mecholsky, R. W. Rice, and S. W. Freiman, "Prediction of Fracture Energy and Flaw Size in Glasses from Measurements of Mirror Sizes," J. Am. Ceram. Soc., vol. 57, 1974, pp. 440-443.

3. J. J. Mecholsky, S. W. Freiman, and R. W. Rice, "Fracture Surface Analysis of Ceramics," J. Mater. Sci., vol. 11, 1976, pp. 1310-1319.

4. J. J. Mecholsky, S. W. Freiman, and R. W. Rice, "Fractographic Analysis of Ceramics," ASTM STP 645, B. M. Strauss and W. H. Cullen, Eds., American Society for Testing and Materials, pp. 363-379, 1978.

5. J. J. Mecholsky and M. G. Drexhage, "Comparison of Optical and Fractographic Measurements of Residual Stress in Compressively Clad Glass Rods," J. Am. Ceram. Soc., vol. 63, 1980, pp. 347-349.

6. D. B. Marshall, B. R. Lawn, and J. J. Mecholsky, "Effect of Residual Contact Stresses on Mirror/Flaw-Size Relations," J. Am. Ceram. Soc., vol. 63, 1980, pp.358-360.

7. S. R. Choi and J. E. Ritter, "Fractographic Analysis of Fused Silica Optical Fibers with Subthreshold Indentation Flaws," Phys. Chem. Glasses, vol. 32, 1991, pp. 79-80.

8. J. W. Johnson and D. G. Holloway, "On the Shape and Size of the Fracture Zones on Glass Fracture Surfaces," Philos. Mag., vol. 14, 1966, pp. 731-743.

9. A. I. A. Abdel-Latif, R. C. Bradt, and R. E. Tressler, "Dynamics of Fracture Mirror Boundary Formation in Glass," Int. J. Fracture, vol. 13, 1977, pp. 349-359.

10. D. K. Shetty, A. R. Rosenfield, and W. H. Duckworth, "Crack Branching in Ceramic Disks Subjected to Biaxial Flexure," J. Am. Ceramic. Soc., vol. 66, 1983, pp. C10 - C12.

11. P. Shi, J. E. Ritter, and K. Jakus, "Effect of Temperature on the Mirror-Mist Constant of Soda-Lime and Boro-silicate Glasses," Phys. Chem. Glasses, vol 30. 1989, pp. 34-35.

12. M. Ramulu, R. C. Bradt, A. S. Kobayashi, and K. H. Yang, "A Dynamic Fracture Mechanics Interpretation of Multiple Mist Regions on Soda-Lime-Silicate Glass Fracture Surfaces, pp. 215-227 in Fractography of Glass and Ceramics, Advanced in Ceramics, vol. 22, edited by J. R. Varner and V. D. Frechette, The American Ceramic Society, 1988.

13. S. R. Choi and J. A. Salem, "Indentation Flaw Formation and Strength Responses of Silicon Nitride Ceramics at Low Indentation Loads," J. Mater. Sci. Lett., vol. 11, 1992, pp. 1398-1400.

14. E. H. Yoffe, "The Moving Griffith Crack," Philos. Mag., vol.42, 1951, pp. 739-750.

15. A. B. J. Clark and G. R. Irwin, "Crack Propagation Behaviors," Exp. Mech., vol. 6, 1966, pp.321-330.

16. H. P. Kirchner and J. W. Kirchner, "Fracture Mechanics of Fracture Mirrors," J. Am. Ceram. Soc., vol. 62, 1979, pp. 198-202.

17. D. K. Shetty, G. K. Bansal, A. R. Rosenfield, and W. H. Duckworth, "Criterion for Fracture-Mirror Boundary Formation in Ceramics," J. Am. Ceram. Soc., vol 63, 1980, pp.106-108.

18. H. P. Kirchner and J. C. Conway, "Criteria for Crack Branching in Cylindrical Rods: II. Flexure," J. Am. Ceram. Soc., vol. 70, 1987, pp. 419-425.

19. "Standard Practice for Fractography and Characterization of Fracture Origins in Advanced Ceramics," ASTM Designation: C1322-96a, American Standards for Testing and Materials, Annual Books of ASTM Standards, vol. 15.01, 1997.

20. S. R. Choi and J. A. Salem, "Elevated-Temperature Slow Crack Growth Testing of a Silicon Nitride in Uniaxial and Biaxial Flexure Loading Conditions," unpublished work, NASA Lewis Research Center, Cleveland, OH, 1997.

21. Data from Oak Ridge National Laboratory, Oak Ridge, TN, 1996.

22. S. R. Choi, J. E. Ritter, and K. Jakus, "Impact/Erosion Testing of Advanced Ceramics," unpublished work, University of Massachusetts, Amherst, 1989.

23. L. M. Powers, J. A. Salem, and S. R. Choi, "Failure Prediction Using the Ring-on-Ring Test and the CARES/LIFE Integrated Design Program," ASME paper # DE-vol.55, Reliability, Stress Analysis, and Failure Prevention, pp. 55-63, ASME, 1993.

24. D. K. Shetty, A. R. Rosenfield, P. McGuire, G. K. Bansal, and W. H. Duckworth, "Biaxial Flexure Test for Ceramics," Ceram. Bull., vol. 59, 1980, pp. 1193-1197.

25. S. R. Choi and J. A. Salem, "Slow Crack Growth of 96 wt % Alumina with Various Specimen/Loading Configurations," unpublished work, NASA Lewis Research Center, Cleveland, OH, 1997.

26. S. R. Choi, unpublished work, NASA Lewis Research Center, Cleveland, OH, 1994.

27. N. N. Nemeth, L. M. Powers, L. A. Janosik, and J. P. Gyekenyesi, "Time-Dependent Reliability Analysis of Monolithic Ceramic Components Using the CARES/LIFE Integrated Design Program," pp. 390-408 in Life Prediction Methodologies and Data for Ceramic Materials, ASTM STP 1201, C. R. Brinkman and S. F. Duffy, Eds., American Society for Testing and Materials, Philadelphia, 1994.

28. S. R. Choi, "Slow Crack Growth Analysis of Finite, Plate Specimens in Constant Stress-Rate Testing," to be submitted for publication, 1997.

29. H. P. Kirchner, "Brittleness Dependence of Crack Branching in Ceramics," J. Am. Ceram. Soc., vol. 69, 1986, pp. 339-342.

30. J. C. Newman and I. S. Raju, "An Empirical Stress-Intensity Factor Equation for the Surface Crack," Eng. Fract. Mech., vol 15, 1981, pp. 185-192.

31. A. Arora, D.B. Marshall, and B.R. Lawn, "Indentation Deformation/Fracture of Normal and Anomalous Glasses," J. Non-Cryst. Solids, vol. 31, 1979, pp 415-428.

TABLE I. —SUMMARY OF FRACTURE MIRROR AND CRACKING BRANCHING CONSTANTS

Number	Material	Type of testing	Loading/specimen configurations	Branch (B) or mirror (M) ?	Hardness H (GPa)	K_{IC}[#] (MPa√m)	A_b or A_m (MPa√m)	A_b/K_{IC} or A_m/K_{IC}
1	NC132 Si$_3$N$_4$ [3][20]	const. stress-rate test;1100 °C	4-pt flexure (20/40mm)/ beams (3mm×4mmx50mm)	M	16.5	4.64[1]	[2]9.40(1.19)	2.03
2	NC132 Si$_3$N$_4$ [20]	const. stress-rate test;1100 °C	ring-on-ring (18.5/40mm) /disks (2mm×45mm)	B	16.5	4.64[1]	5.66(1.49) [1]7.92(2.08)	1.22 1.71
3	GN10 Si$_3$N$_4$ [21]	RT strength	Tension/ORNL tension	M	14.5	5.23[1]	11.78(1.41)	2.25
4	GN10Si$_3$N$_4$ [22]	RT post-impact strength	ring-on-ring (12.7/28.6mm) /disks (2mm×40mm)	B	16.4	4.6[1]	10.32	2.23
5	Hexoloy SiC [23]	RT strength	ring-on-ring (11.5/23mm)/ plates (2mmx25mmx25mm)	B	27.0	2.41[1]	5.45(0.30)	2.26
6	96wt% Al$_2$O$_3$ [25]	RT const. stress-rate test	ring-on-ring (11.3/20.7mm)/ plates (2mm×25mm×25mm)	B	10.0	3.10[1]	7.24(0.66)	2.34
7	96wt% Al$_2$O$_3$ [25]	RT const. stress-rate test	ball-on-ring (20.58mm)/ plates (2mm×25mm×25mm)	B	10.0	3.10[1]	7.39(0.55)	2.38
8	96wt% Al$_2$O$_3$ [25]	RT const. stress-rate test	4-pt flexure (20/40mm)/ beams (3×4×50mm)	M	10.0	3.10[1]	7.64(0.53)	2.46
9	Y-TZP [22]	RT post-impact strength	ring-on-ring (12.7/28.6mm)/ disks (2mm×40mm)	B	10.9	5.49[2]	11.48(1.46)	2.09
10	AS44 Si$_3$N$_4$ [22]	RT post-impact strength	ring-on-ring (12.7/28.6mm)/ disks (2mm×40mm)	B	15.6	5.78[2]	10.85(2.71)	1.88
11	SN220 Si$_3$N$_4$ [22]	RT post-impact strength	ring-on-ring (12.7/28.6mm)/ disks (2mmx40mm)	B	13.0	4.81[2]	8.13(2.36)	1.69
12	Norton mono Si$_3$N$_4$ [13]	RT strength	4-pt flexure (4.8/20mm)/ beams (3mm×4mm×25mm)	M	16.7	3.90[3]	5.88(0.14)	1.51
13	Norton comp SiC$_w$/Si$_3$N$_4$ [13]	RT strength	4-pt flexure (4.8/20mm)/ beams (3mm×4mm×25mm)	M	19.5	4.64[3]	6.63(0.11)	1.43
14	Fused silica glass [26]	RT strength	4-pt flexure (20/40mm)/ rods (2mm and 4mm in dia.)	M	7.6	0.79[4]	2.20(0.33)	2.78
15	Soda-lime glass [27]	RT const. stress-rate test	ring-on-ring (10/32.2mm)/ plates (1.5mm×50mm×50mm)	M	5.6	0.75[4]	1.81(0.28)	2.41
16	Fused silica optical glass fibers [7]	RT const. stress-rate test	tension/ fibers (150μm in dia.)	M	7.6	0.79[4]	2.10	2.66
17	Soda-lime glass [28]	RT const. stress-rate test	4-pt flexure (20/40mm)/plates (1.2mm×25mm×75mm)	B	5.6	0.76[3]	3.54(0.64)	4.65

Notes: [#] Fracture toughness evaluated with 1) SEPB method (ASTM PS070); 2) Indentation fracture method; 3) Indentation strength method; and 4) from reference 31.

[1]Corrected using a correction factor of 1.38 (see Section III-4).

[2]The number in parenthesis indicates ±1.0 standard deviation.

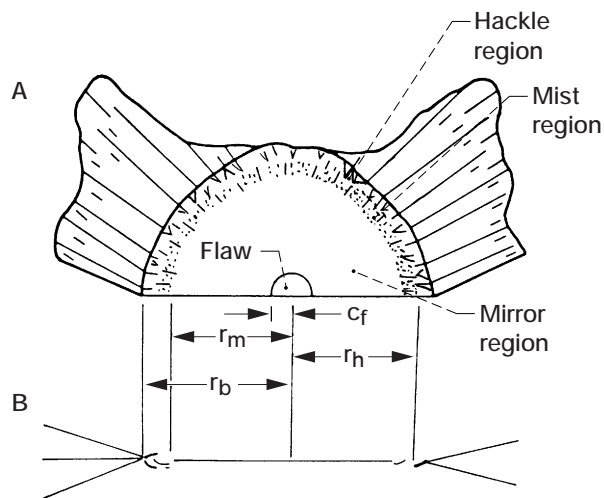[3]The number in parenthesis represents corresponding reference.

Figure 1.—Schematic of fracture mirror, mist, hackle, and branching patterns on typical ceramic fracture surface [1]: c_f represents the critical flaw size, and r_m, r_h, and r_b represent the fracture mirror size, hackle length, and crack branching length, respectively. A fracture surface and a crack branching pattern represent in A and B, respectively.
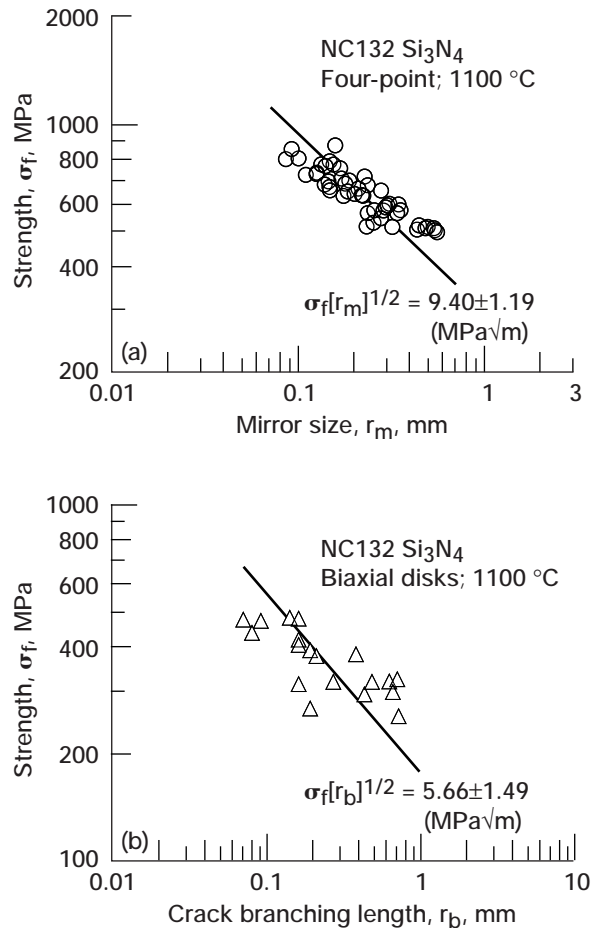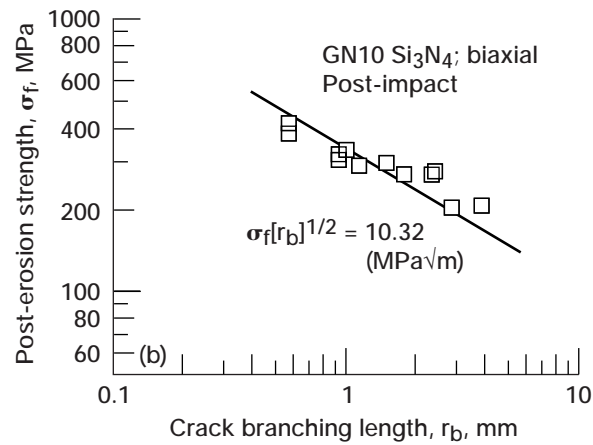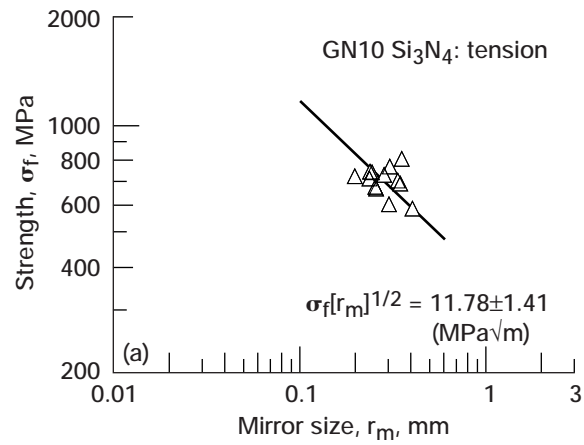

Figure 2.—Fracture strength as a function of fracture mirror size (a) and crack branching length (b) for NC132 silicon nitride tested in constant stress-rate testing at 1100 °C in air [20]: (a) four-point uniaxial flexure; (b) ring-on-ring biaxial flexure. The lines represent the best-fit lines based on Eq. (1).
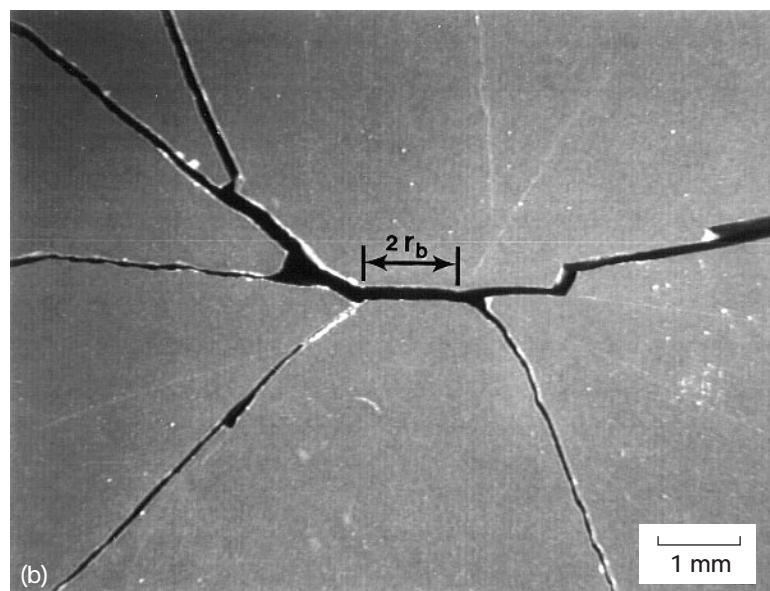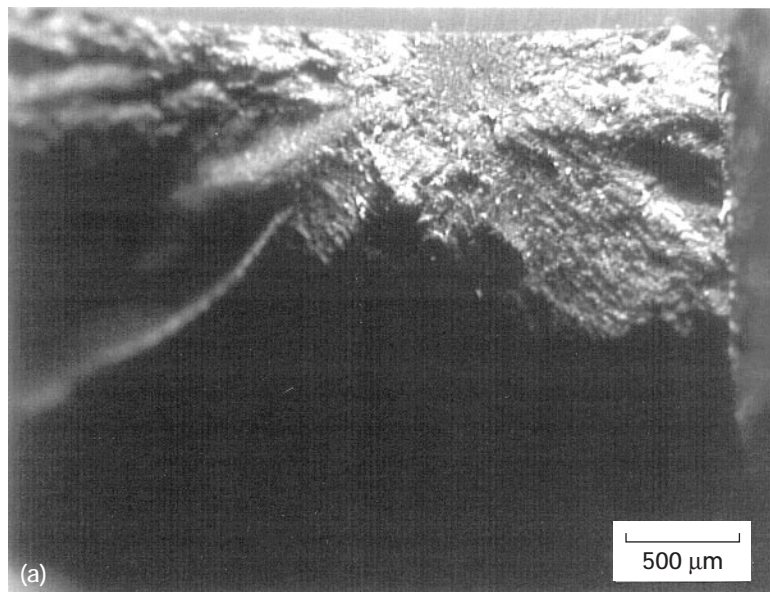
Figure 3.—A typical fracture surface (a) and a typical crack branching pattern (b) of NC132 silicon nitride tested in constant stress-rate testing at 1100 °C in air [20]: (a) four-point uniaxial flexure; (b) ring-on-ring biaxial flexure.

Figure 4.—Fracture strength as a function of fracture mirror size (a) and crack branching length (b) for GN10 silicon nitride tested at room temperature: (a) pure tension [21]; (b) post-impact strength in ring-on-ring biaxial flexure [22].
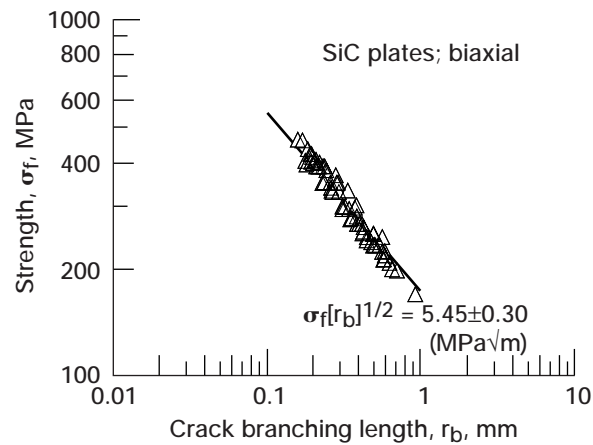
Figure 5.—Fracture strength as a function of crack branching length for Hexoloy silicon carbide plates tested in ring-on-ring biaxial flexure at room temperature [23].

(a)

1 mm

(b)

Flaw

500 µm
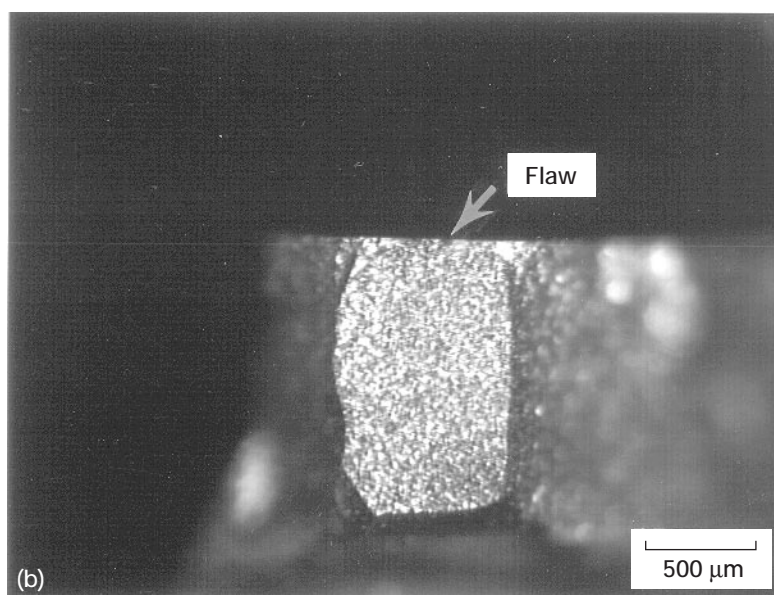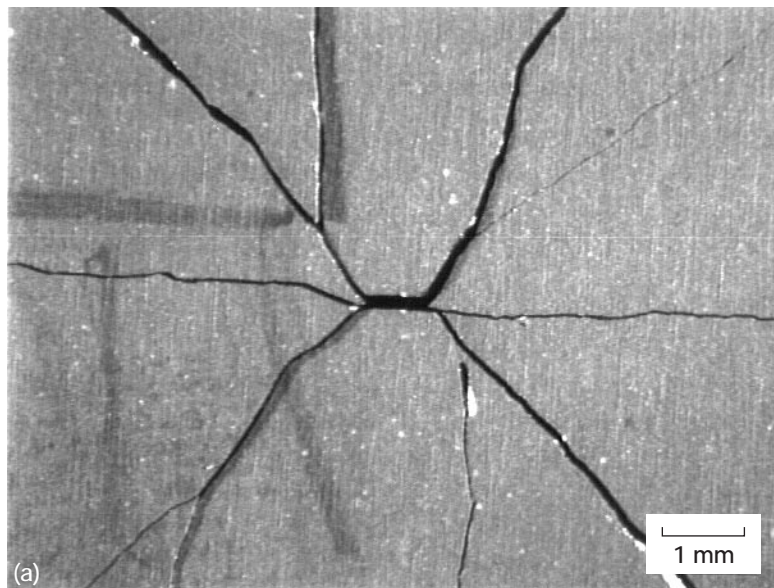
Figure 6.—A typical crack branching pattern and corresponding fracture surface of a Hexoloy silicon carbide plate tested in ring-on-ring biaxial flexure at room temperature [23].
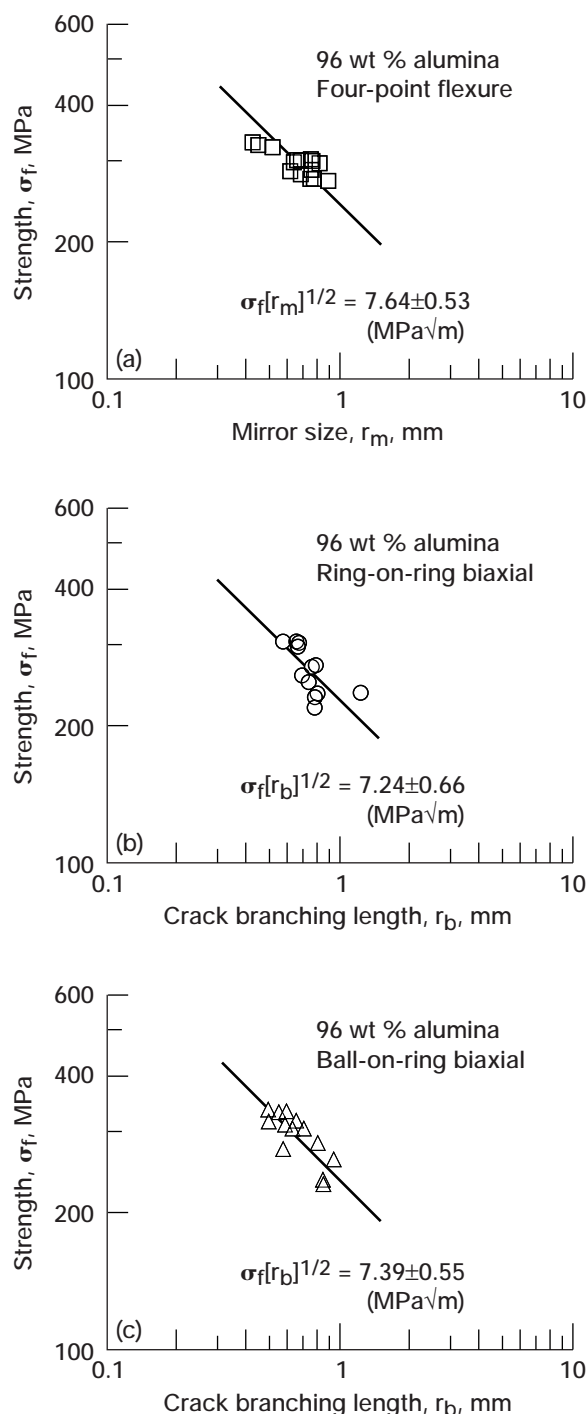
Figure 7.—Fracture strength as a function of fracture mirror size (a) and crack branching length (b) and (c) for 96 wt % alumina (Alsimag) tested in constant stress-rate testing at room temperature [25]: (a) four-point flexure; (b) ring-on-ring biaxial flexure; (c) ball-on-ring biaxial flexure.
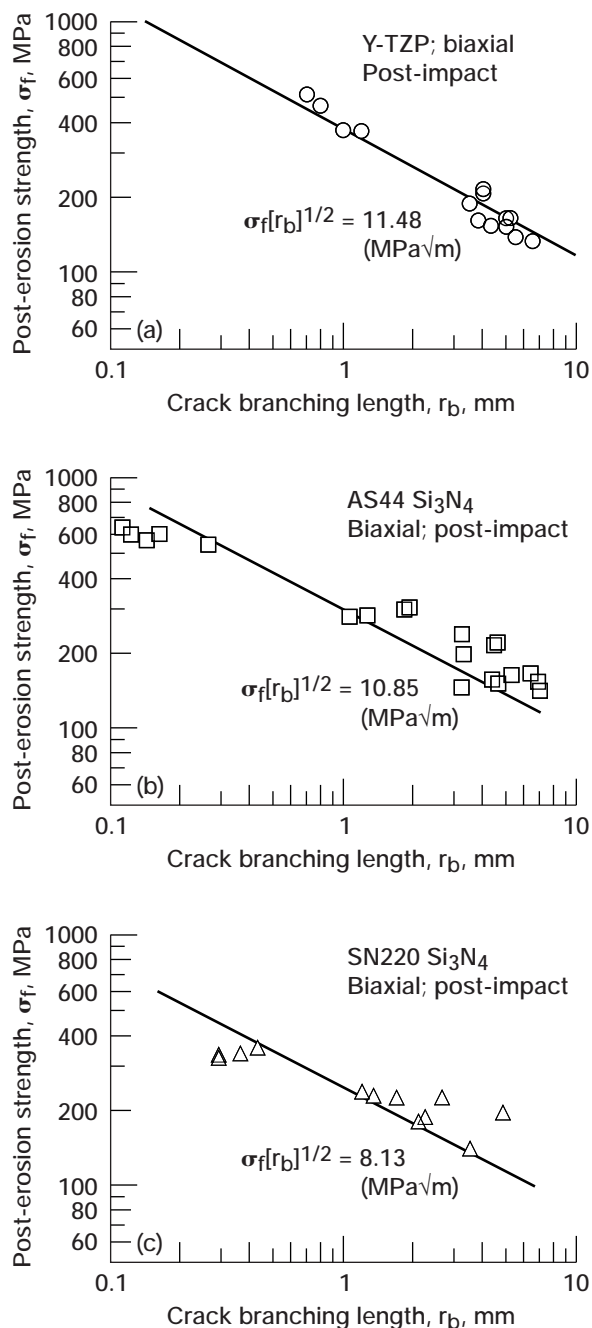
Figure 8.—Post-impact strength as a function of crack branching length for Y-TZP and AS44 and SN220 silicon nitride disk specimens tested in ring-on-ring biaxial flexure [22]: (a) Y-TZP; (b) AS44 silicon nitride; (c) SN220 silicon nitride.

15
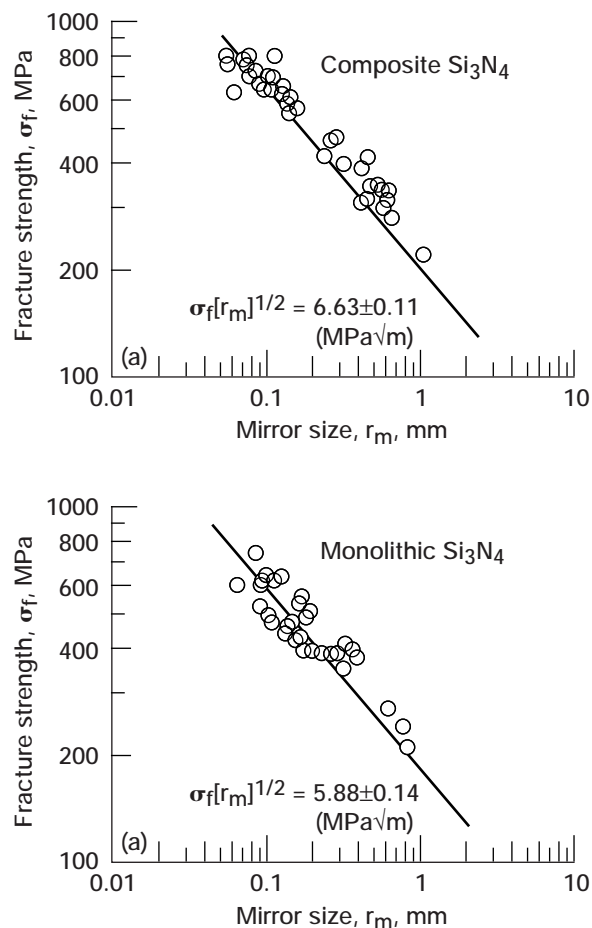
Figure 9.—Fracture strength as a function of fracture mirror size for 30 vol % SiC whisker-reinforced composite silicon nitride (a) and similar monolithic silicon nitride (b) tested in four-point uniaxial flexure at room temperature [13].
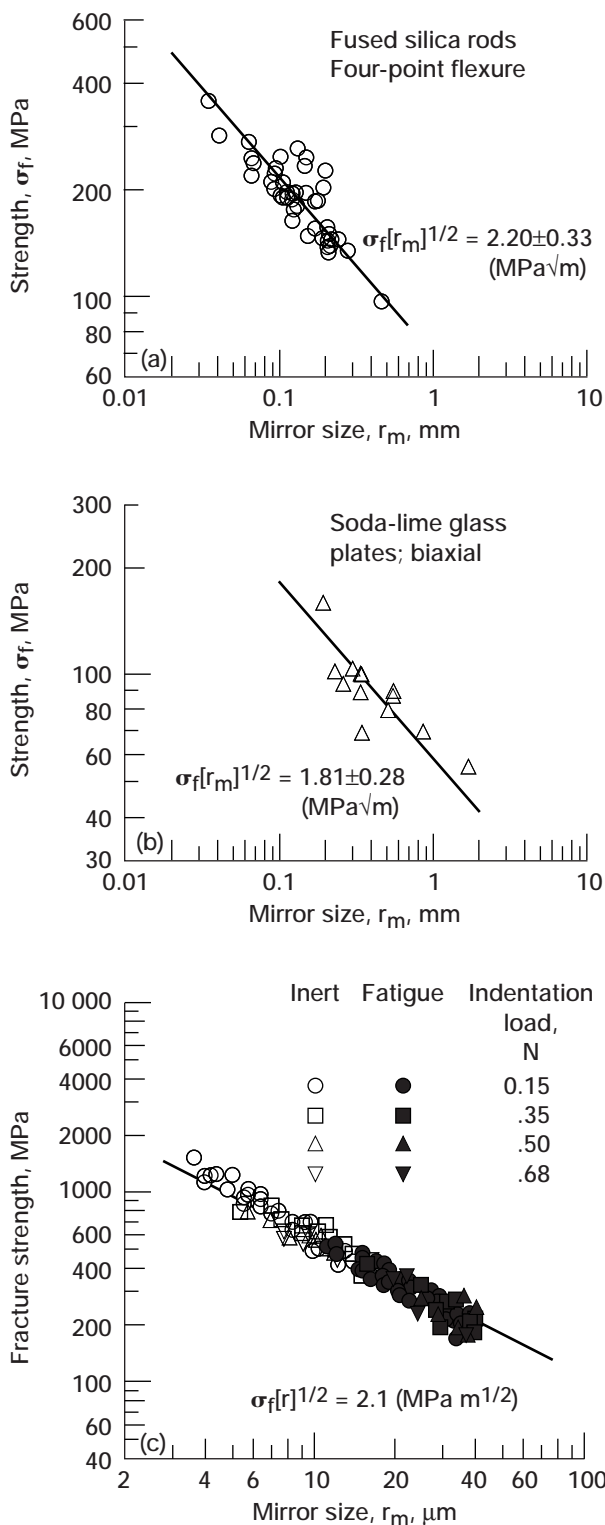

Figure 10.—Fracture strength as a function of fracture mirror size for glasses tested at room temperature: (a) as-received fused silica glass rods in four-point uniaxial flexure [26]; (b) etched soda-lime glass plates in ring-on-ring biaxial flexure [27]; (c) indented fused silica optical glass fibers in pure tension [7].
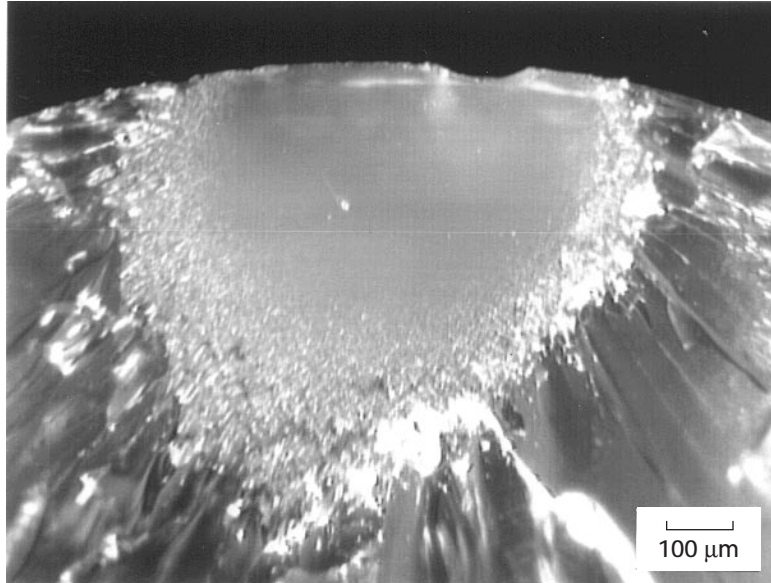
Figure 11.—A typical fracture surface of a fused silica glass rod showing a well-defined fracture mirror formation.
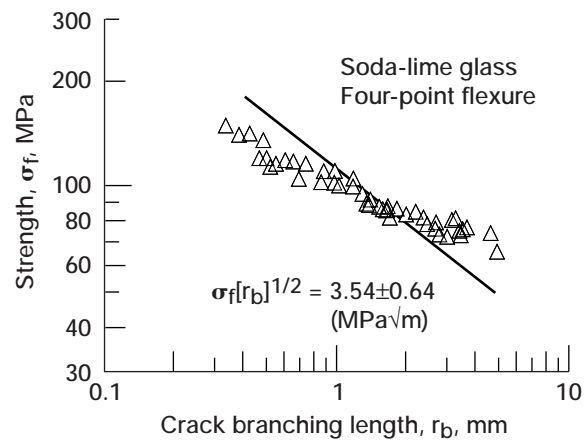

Figure 12.—Fracture strength as a function of crack branching length for indented soda-lime micro-slide plates tested in constant stress-rate testing in four-point uniaxial flexure at room temperature [28].
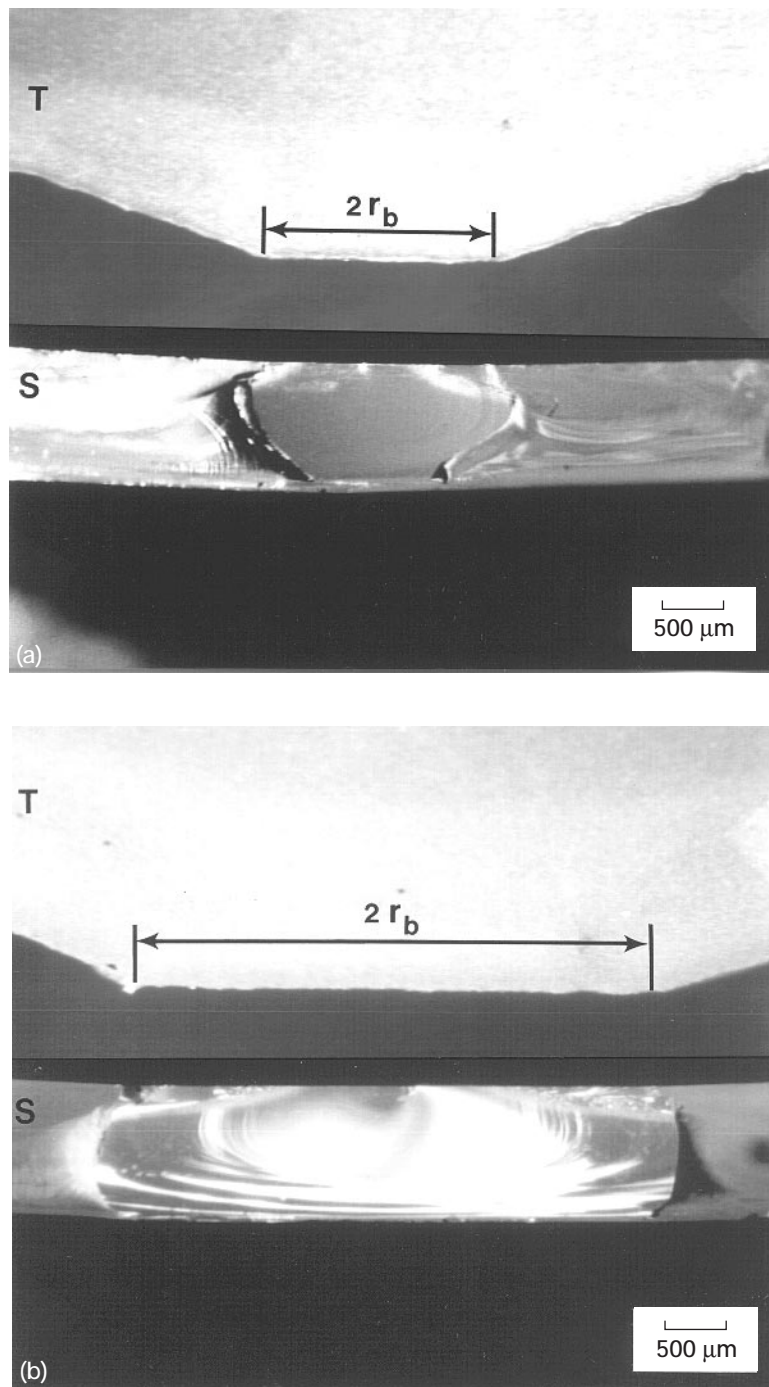
Figure 13.—Typical crack branching patterns and corresponding fracture surfaces of indented soda-lime glass plates tested in constant stress-rate testing in four-point uniaxial flexure at room temperature: (a) high failure stress; (b) low failure stress. T and S represent top view and side view (fracture surface), respectively.
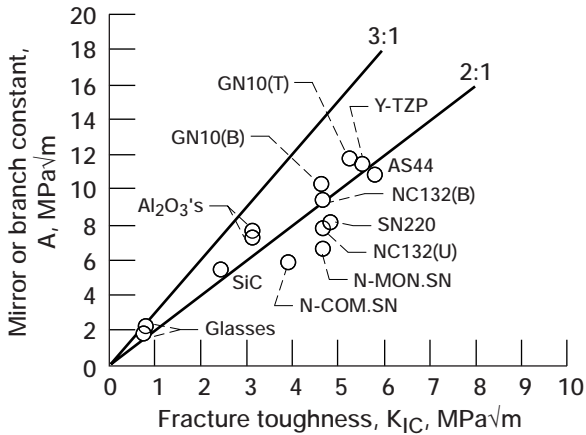
Figure 14.—Plots of fracture mirror or crack branch-
ing constant as a function of fracture toughness
for the materials studied in this work, except for
the soda-lime glass crack branching data (Figure
12). The NC132 fracture mirror constant was
corrected using a correction factor of 1.38 (see
Section 4). T, B and U denote pure tension, biaxial
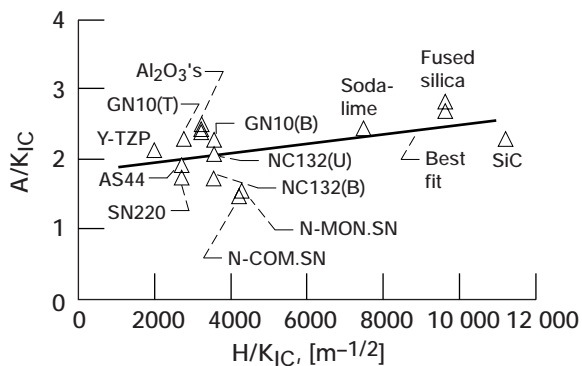and uniaxial flexure loadings, respectively.

Figure 15.—Plots of A/K_{IC} as a function of H/K_{IC} for
the materials studied in this work, except for the
soda-lime glass crack branching data (Figure 12).
The line represents a best-fit line based on a
relation of A/K_{IC} vs. H/K_{IC}, which is $A/K_{IC} =$
$6.76 \times 10^{-5} H/K_{IC} + 1.8055$ (units in all MPa and m).
T, B and U denote pure tension, biaxial and
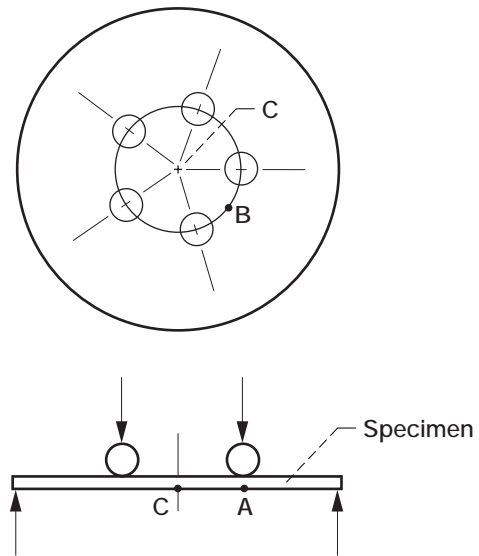uniaxial flexure loadings, respectively.

Figure 16.—Geometry of a disk specimen
in ring-on-ring biaxial flexure used for
NC132 silicon nitride disk specimens
tested in constant stress-rate testing at
1100 °C in air [20]. The regions A, B and
C denote at the tensile side of a disk
specimen: region A - directly under the
loading ball; region B - between the two
adjacent loading balls; region C - at the
center.

REPORT DOCUMENTATION PAGE

Public reporting burden for this collection of information is estimated to average 1 hour per response, including the time for reviewing instructions, searching existing data sources, gathering and maintaining the data needed, and completing and reviewing the collection of information. Send comments regarding this burden estimate or any other aspect of this collection of information, including suggestions for reducing this burden, to Washington Headquarters Services, Directorate for Information Operations and Reports, 1215 Jefferson Davis Highway, Suite 1204, Arlington, VA 22202-4302, and to the Office of Management and Budget, Paperwork Reduction Project (0704-0188), Washington, DC 20503.

1. AGENCY USE ONLY (Leave blank)	2. REPORT DATE	3. REPORT TYPE AND DATES COVERED
	February 1998	Technical Memorandum

4. TITLE AND SUBTITLE

Crack Branching and Fracture Mirror Data of Glasses and Advanced Ceramics

6. AUTHOR(S)

Sung R. Choi and John P. Gyekenyesi

5. FUNDING NUMBERS

WU–523-22-13-00

7. PERFORMING ORGANIZATION NAME(S) AND ADDRESS(ES)

National Aeronautics and Space Administration
Lewis Research Center
Cleveland, Ohio 44135–3191

8. PERFORMING ORGANIZATION REPORT NUMBER

E–11019

9. SPONSORING/MONITORING AGENCY NAME(S) AND ADDRESS(ES)

National Aeronautics and Space Administration
Washington, DC 20546–0001

10. SPONSORING/MONITORING AGENCY REPORT NUMBER

NASA TM—1998-206536

11. SUPPLEMENTARY NOTES

Sung R. Choi, Cleveland State University, Cleveland, Ohio 44115 and NASA Senior Resident Research Associate at Lewis Research Center and John P. Gyekenyesi, NASA Lewis Research Center. Responsible person, John P. Gyekenyesi, organization code 5920, (216) 433–3210.

12a. DISTRIBUTION/AVAILABILITY STATEMENT

Unclassified - Unlimited
Subject Category: 27   Distribution: Nonstandard

This publication is available from the NASA Center for AeroSpace Information, (301) 621–0390.

12b. DISTRIBUTION CODE

13. ABSTRACT (Maximum 200 words)

The fracture mirror and crack branching constants were determined from three glasses and nine advanced ceramics tested under various loading and specimen configurations in an attempt to use the constants as a data base for fractography. The ratios of fracture mirror or crack branching constant to fracture toughness were found to be approximately two for most ceramic materials tested. A demonstration of how to use the two constants as a tool for verifying stress measurements was presented for silicon nitride disk specimens subjected to high-temperature, constant stress-rate biaxial flexure testing.

14. SUBJECT TERMS

Glass; Advanced ceramics; Fractography; Fracture mirror; Crack branching; Fracture mirror constant; Crack branching constant

15. NUMBER OF PAGES
25

16. PRICE CODE
A03

17. SECURITY CLASSIFICATION OF REPORT	18. SECURITY CLASSIFICATION OF THIS PAGE	19. SECURITY CLASSIFICATION OF ABSTRACT	20. LIMITATION OF ABSTRACT
Unclassified	Unclassified	Unclassified	